scientific reports

Check for updates

OPEN

Topology optimization of wheel spoke cavities for lightweight design under bending fatigue and impact load cases

Guangdong Zhang[1]✉, Xin Cui[1], Yongxing Zang[2]✉, Yangyang Zhou[3], Jianjun Lu[2], Zhansheng Li[2], Haitao Yang[2], Jiandong Wang[2], Zhen Ye[2], Risheng Li[2] & Linzhen Zhou[1]

This paper presents a Multi-Load-Case topology optimization framework for aluminum alloy wheels to overcome the limitations of empirical rear-cavity lightweight designs. To balance structural integrity and mass reduction without altering the aerodynamic outboard styling, a region-constrained topology optimization was conducted. By employing a compromise programming method based on strain energy ratios, the weighting coefficients for bending fatigue and 13° impact load cases were scientifically calibrated. Furthermore, manufacturing constraints, including a 10 mm minimum member size and draw directions, were incorporated to ensure direct compatibility with conventional casting. The results demonstrate that the optimized depth-gradient cavities successfully reduced the peak von Mises stress for bending fatigue by 19.25% (from 133.9 to 108.13 MPa) and for the 13° impact by 14.57% (from 74.63 to 63.76 MPa), alongside a slight mass reduction of 0.53%. This approach offers a mathematically rigorous and industrially viable paradigm for the multi-objective lightweight design of high-performance automotive components.

Keywords Spoke weight reduction cavity, Topology optimization, Bending fatigue, 13° impact

As global environmental policies become rigorous, the automotive industry faces intensified pressure to achieve energy conservation and emission reduction targets[1]. Empirical studies reveal that a 10% reduction in vehicle mass can simultaneously extend driving range by 5%–6% while reducing energy consumption by 6%–8%. Specifically, this weight reduction corresponds to an equivalent decrease in CO_2 emissions by 6%–8%[2]. These synergistic benefits establish lightweight design as an essential strategy for overcoming energy consumption constraints in both conventional and electric vehicles.

As a critical component of the unsprung mass, the wheel is the primary load-bearing interface between the vehicle and ground transmission system, fundamentally determining handling stability and ride comfort. Industry studies demonstrate a 10–15 kg sprung mass reduction equivalency for each 1 kg unsprung mass reduction in wheels – a mass reduction effectiveness 12 times higher than non-rotating components[3].

While the general pursuit of lightweight wheels often targets substantial mass reduction, practical engineering must frequently prioritize structural safety and design compliance over extreme lightweighting, especially for components that initially fail dynamic safety tests. Current design approaches primarily involve three strategies: material innovation, structural optimization through advanced simulation methods, and manufacturing process enhancement. Compared with conventional lightweighting strategies wheel topology optimization uses mathematical methods to achieve the optimal balance between structure and performance. It has the advantages of high material utilization, multi-objective coordination, and innovative conceptual design, and it has been widely used in wheel lightweight design.

In recent years, researchers have conducted extensive studies in topology optimization[4–12]. Regarding wheel topology optimization, significant progress has been made in balancing lightweight design and structural performance. Early single-objective studies prioritized static stiffness in aluminum wheels (Zhang et al.[13], while later multi-objective frameworks balanced bending stiffness and modal frequency (Xiao et al.[14], 13.5%

[1]School of Mechanical Engineering, Yancheng Institute of Technology, Yancheng 224051, Jiangsu, China. [2]Hebei High Strength and Toughness Lightweight Wheel Technology Innovation Center, Baoding Lizhong Wheel Manufacturing Co., Ltd., Baoding 071000, Hebei, China. [3]Hebei Provincial Engineering Research Center for Recycled Aluminum Alloy Automotive Parts Manufacturing, Baoding Lizhong Dong'an Light Alloy Components Manufacturing Co., Ltd., Baoding 071100, Hebei, China. ✉email: gdzhang@ycit.edu.cn; xuliandi@lzwheel.com

weight reduction). Recent advances integrate complex load cases (e.g., Wang et al.'s 13°/90° impact-constrained model[15] and Multiphysics coupling (Kim et al.'s frequency-mass optimization[16]. Material innovations further spurred methodologies like carbon-fiber/magnesium alloy co-design (Chu et al.[17] and hierarchical hybrid optimization (Zhang et al.[18], 21.6% mass reduction). Despite these progress, existing approaches universally reconstruct the entire spoke morphology, disregarding pre-existing styling constraints and consumer-driven design requirements.

Beyond the specific domain of wheel spokes, the topology optimization of high-performance components must be situated within the broader context of advanced high-fidelity simulation and multi-objective optimization. Recent advancements have demonstrated that transitioning from simplified variable-density maps to functional structures requires rigorous high-fidelity finite element modeling (FEM) and dynamic analysis protocols to accurately capture transient structural responses[19]. Furthermore, the optimization of complex geometries—such as those explored in GFRP fabric pultrusion panels[20], innovative carbon fiber-reinforced composite sandwich panels[21], and hybrid structures with multilayer panels[22]—highlights the critical necessity of meticulously balancing material distribution with structural stiffness. These cross-disciplinary perspectives provide valuable theoretical foundations for justifying the weighting factors and Multi-Load-Case trade-offs in structural optimization. Finally, to ensure long-term operational safety, the optimized structures must be validated through established fatigue life evaluation techniques[23] and dynamic stress analysis[24]. Such methodologies are essential for verifying that the introduction of mass-reduced cavities does not induce critical stress concentrations, which could otherwise lead to premature failure under cyclic bending loads.

However, a critical gap remains in current wheel topology optimization research. Extant studies predominantly focus on full-area topological approaches that designate the entire spoke as the design domain. While this comprehensive optimization strategy theoretically maximizes material efficiency, it fundamentally reconstructs the spoke's morphological features. This process inevitably compromises the aesthetic integrity of the design and disregards consumer-driven, pre-existing styling requirements.

To address these limitations, this study proposes a region-constrained optimization framework for wheels that fail to meet the standardized bending fatigue and 13° impact tests. The innovative methodology confines the topological domain to specific inboard regions (rear cavities) of the spokes while preserving their original outboard styling. This dual-load-case optimization scheme integrates bending fatigue and 13° impact loading scenarios, employing a compromise programming approach based on strain energy ratios to formulate a weighted evaluation function that balances multiple operational requirements. The proposed technique demonstrates superior computational efficiency compared to conventional methods while maintaining structural safety, successfully providing a practical engineering solution that balances structural safety compliance with strict appearance preservation. This sector-specific optimization strategy achieves targeted material redistribution in the spoke's weight-reduction cavity, particularly enhancing energy absorption characteristics critical for impact resistance.

Theoretical framework and baseline modeling

Mathematical formulation of the SIMP method

Topology optimization is a systematic computational approach that determines the optimal material distribution within a specified design domain to maximize structural performance under prescribed load cases and constraints[25]. As an effective tool for structural lightweight design, this methodology has been extensively implemented in various engineering applications. Currently established topology optimization techniques primarily include three categories: the homogenization method[25], evolutionary structural optimization[26], and the level set method[27]. The variable-density method has gained significant popularity in engineering practice, due to its computational efficiency and simplified implementation[28].

The fundamental principle of the variable-density method involves introducing a pseudo-density field to characterize material distribution, where each finite element's relative density serves as the design variable. The variable-density method transforms the discrete topology optimization problem into a continuous material distribution problem. The technique employs the Solid Isotropic Material with Penalization (SIMP) interpolation model[29], which establishes a power-law relationship between material elasticity modulus and element density by introducing a penalization exponent p. Specifically, the SIMP model penalizes intermediate densities ($0 < \rho_i < 1$) through the function ρ_i^p, with $p \geqslant 3$to effectively drive the density distribution toward 0–1 solutions.

The SIMP material interpolation relationship is explicitly defined as follows:

$$E_i(\rho_i) = E_{\min} + \rho_i^p (E_0 - E_{\min}), \rho_i \in [0, 1] \tag{1}$$

where ρ_i represents the design variable, defined as the relative density of the material, with $\rho_i = 1$indicating solid material and $\rho_i = 0$indicating void; p denotes the power-law penalty exponent ($p \geqslant 3$); E_i is the elastic modulus of the element; E_0 and $E_{\min}$ define the elastic moduli of fully dense and void materials, respectively, with $E_{\min} = 10^{-9} E_0$to prevent stiffness matrix singularity.

The SIMP-based topology optimization framework is expressed through the following mathematical formulation:

$$\begin{cases} \text{find } \rho = (\rho_1, \cdots, \rho_n) \\ \min\ C(\rho) = U^T K U = \sum_{i=1}^{n} (\rho_i)^p u_i^T K_i u_i \\ \text{subject to } K(\rho)U = P \\ V(\rho) \leqslant f \cdot V_0 \\ 0 = \rho_{\min} \leqslant \rho_i \leqslant 1 \end{cases} \tag{2}$$

where $C(\rho)$denotes structural compliance; q denotes the penalty factor, $q > 1$; $\rho_{\min}$is the minimum relative density value, $\rho_{\min} = 0$to enable void regions; U corresponds to the global displacement vector; K signifies the global stiffness matrix; $u_i$represents the element displacement vector; $K_i$is the element stiffness matrix; P denotes the load vector; V represents the optimized volume; $V_0$is the initial volume; f corresponds to the maximum volume fraction constraint for optimization.

Baseline finite element modeling and material properties

A finite element wheel model conforming to ISO 4000-2 specifications (18 × 8.5 J configuration) was developed in the Altair HyperMesh® pre-processing environment. The geometric model of the aluminum alloy wheel was discretized using quadratic tetrahedral elements (CTETRA type) with a nominal global sizing of 5 mm. To ensure computational accuracy and eliminate potential stress singularities, rigorous element quality criteria—including skewness, aspect ratio, and Jacobian ratio—were evaluated during the meshing process. Any initial elements exhibiting suboptimal quality at critical stress-concentration zones, particularly the spoke-rim junctions, were systematically corrected. As illustrated in Fig. 1, the corrected mesh ensures smooth geometric transitions and confirms the complete absence of distorted elements. Following these strict quality refinements, a high-fidelity computational grid comprising 329,502 elements and 535,593 nodes was successfully generated.

To accurately capture the high stress gradients across the complex curved surfaces of the wheel spokes and to prevent the shear locking effects commonly associated with first-order elements, second-order 10-node tetrahedral elements were exclusively employed for meshing the wheel model in both the bending fatigue and 13° impact simulations. Combined with the refined 5 mm mesh size, this higher-order element formulation ensures high-fidelity stress evaluation, which is crucial for the subsequent topology optimization and fatigue compliance assessment.

To ensure the accuracy and reliability of the finite element analysis, a mesh sensitivity study was conducted on the baseline wheel model prior to topology optimization. The global element size was sequentially refined (e.g., from 5 mm to 3 mm and then to 2 mm), and the peak von Mises stress and maximum displacement under both bending fatigue and 13° impact load cases were monitored. The results indicated that when the element size was reduced from 5 mm to 3 mm, the change rate of the peak stress and displacement was less than 5%, demonstrating stable convergence. Considering the balance between computational accuracy and solving efficiency, a baseline element size of 5 mm (with localized refinements in critical areas) was ultimately adopted for all subsequent simulations.

The wheel specimen was fabricated from A356.2 cast-aluminum alloy, exhibiting fundamental mechanical properties of $\rho = 2700$ kg/m³ density, $E = 71$ GPa elastic modulus, and $\nu = 0.33$ Poisson's ratio. The material's stress-strain behavior was experimentally determined via uniaxial tensile testing in compliance with ISO 6892-1 standards, with the corresponding stress-strain relationship depicted in Fig. 2. Mechanical characterization revealed yield strength (YS) and ultimate tensile strength (UTS) values of 200 MPa and 250 MPa under as-cast conditions. The design-allowable stress $\sigma_a$for wheel applications was derived through the following mechanical relationship:

$$\sigma_a = \frac{\sigma_b}{n} \tag{3}$$

where$\sigma_b$denotes material yield strength; n is the safety factor, taken as 1.5. Thus, the allowable stress is calculated as: $\sigma_a = 133.3$ MPa.

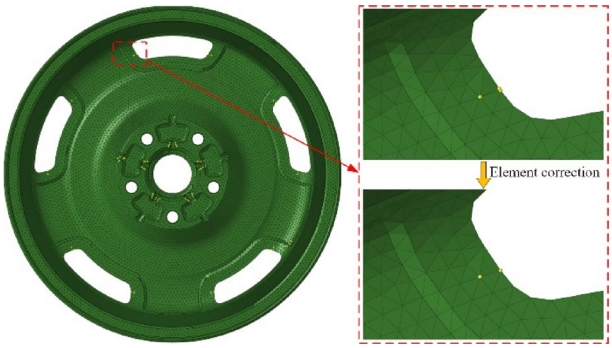

Fig. 1. The element correction at the spoke-rim junctions.

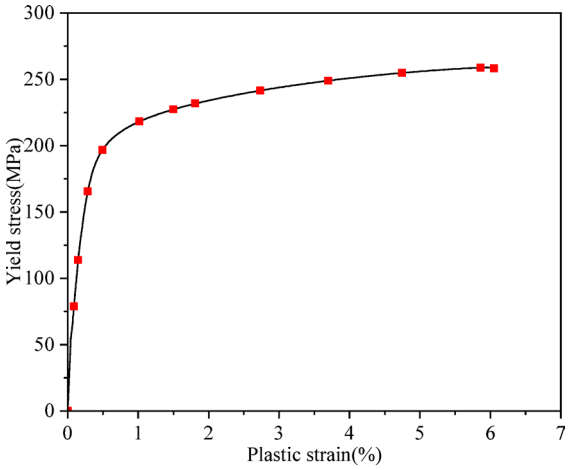

Fig. 2. Stress-strain curve.

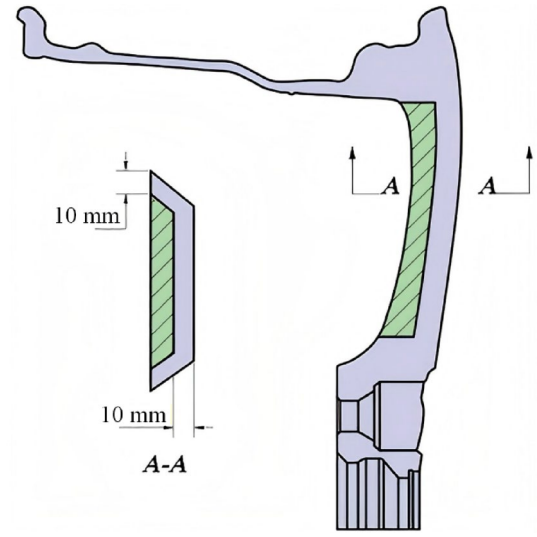

Fig. 3. Weight reduction cavities on the wheel spoke.

Definition of the design domain

The structural design of the spoke rear cavity follows a systematic approach guided by the aerodynamic profile of the wheel's outboard styling curves in conjunction with the brake caliper clearance to define the optimal rear cavity profile precisely. Strategically positioned weight reduction cavities are integrated into the spoke's rear geometry, achieving an optimal balance between mechanical performance and mass reduction goals. Drawing from established casting manufacturing protocols, critical dimensional constraints include maintaining a minimum 10 mm material thickness between the cavity floor and spoke outboard surface, with equivalent 10 mm sidewall specifications throughout the cavity structure. The parametric design space for these weight-optimized cavities is comprehensively illustrated in Fig. 3.

Standardized load cases and boundary conditions

The dynamic bending fatigue performance of the wheel was evaluated following GB/T 5334 – 2021 ("Passenger Car - Wheels - Performance Requirements and Test Methods for Bending and Radial Fatigue Tests")[30], a Chinese national standard modified from ISO 3006:2015. As specified by the standard, all automotive wheels must satisfy the prescribed cyclic loading requirements under simulated cornering conditions. The experimental setup and loading configuration for this fatigue assessment are described in Fig. 4.

F is applied perpendicular to the terminal end of the loading axis to generate static-equivalent bending moment excitation. The wheel assembly undergoes rotational deformation under sustained bending load cases (275,000 cycles) with the following pass/fail criteria:

1. No detectable crack propagation from non-destructive inspection (per GB/T 5334 – 2021 Sect. 6.1.4).
2. Loading point displacement increment ≤ 10% of initial deflection.

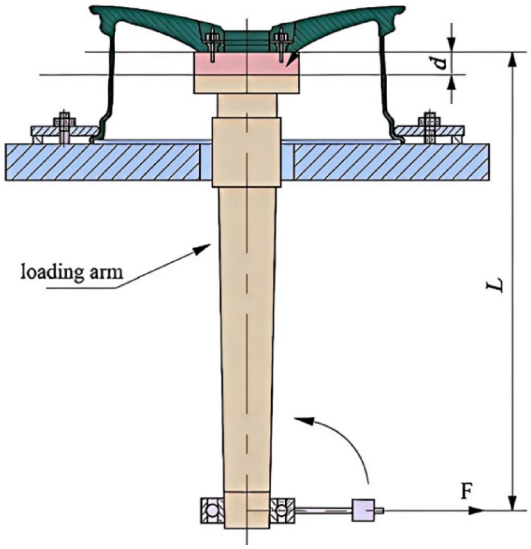

Fig. 4. Setup of bending fatigue test.

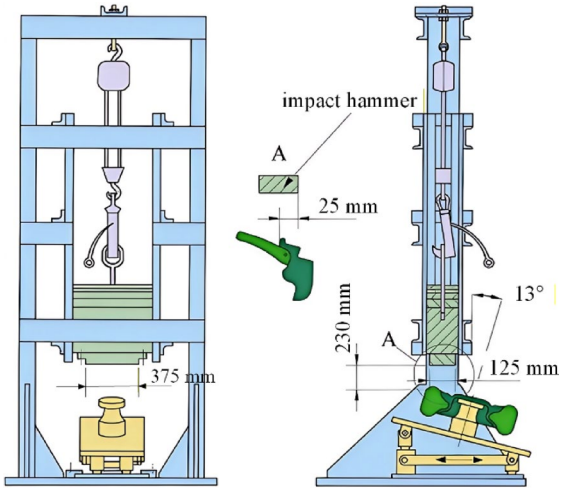

Fig. 5. 13° Impact test.

The bending moment M and loading force F are determined through the following standardized empirical formulas:

$$M = (\mu R + d)FvS \tag{4}$$

$$F = \frac{M}{L} \tag{5}$$

where: μ denotes the prescribed tire-road friction coefficient (0.7); R represents the maximum static loaded radius of the specified tire (0.353 m); d corresponds to the wheel offset (0.045 m); F_v signifies the manufacturer-defined vertical rated load (11145.6 N); S is the fatigue test strengthening coefficient (1.6). L is the loading arm length (1 m);

The bending moment M and the loading force F were calculated as 5,209 N·m and 5,209 N, respectively, using Eqs. (4) and (5).

According to GB/T 15,704 – 2012 "Road vehicles - Light alloy wheels - Impact test procedure" (ISO 7141:2005, IDT)[31], wheels must satisfy the prescribed 13° impact test requirements. This laboratory test method evaluates the wheel's axial impact resistance against curbs through controlled 13°±1° oblique impacts at 230 ± 2 mm height, as schematically represented in Fig. 5.

During the 13° impact test, the wheel-tire assembly shall be mounted on the testing platform with the wheel axis inclined at 13°±1° relative to the vertical orientation. The hammer must be positioned at 230 ± 2 mm above

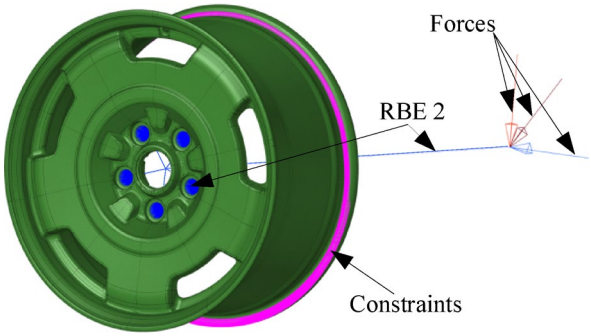

Fig. 6. The finite element model for bending fatigue.

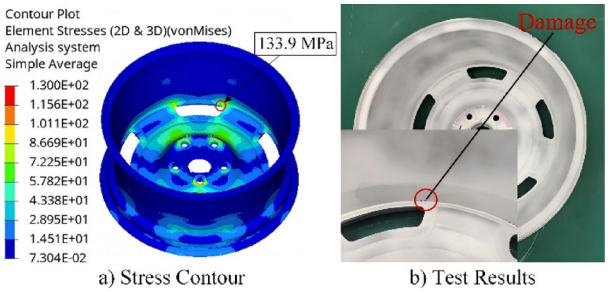

Fig. 7. Bending fatigue simulation and test.

the rim's highest point and shall overlap the rim flange by 25 ± 1 mm. Upon release of the hammer, the following post-impact validation criteria must be satisfied: (a) absence of through-section fractures in the central wheel member; (b) integrity preservation between the central member and rim interface; (c) retention of pneumatic pressure without complete depletion within the 60-second observation period.

The hammer mass (m) shall be determined from the formula:

$$m = 0.6W + 180 \tag{6}$$

where W is the maximum static wheel load specified by the wheel/vehicle manufacturer in kilograms (850 kg), and m is the hammer mass in kilograms (690 kg).

Optimization process and results discussion

Baseline performance evaluation and experimental validation

According to the dynamic bending fatigue test specifications for wheels, all degrees of freedom (DOFs) at nodes along the inner rim edge were constrained. A rigid RBE2 element simulates bolted joints between the loading arm and wheel mounting surface. This five-spoke wheel configuration maintains 72° angular spacing between adjacent spokes. To comprehensively assess stress distributions across the valve window and spoke regions, three distinct loading orientations were implemented at the rigid loading shaft end with a 5209 N force application:

Force (Orientation 1). Direct alignment with the valve hole.

Force (Orientation 2). 36° rotational offset aligning with the spoke central axis.

Force (Orientation 3). 90° rotational offset positioning at spoke-window junctions.

The experimental loading configurations are schematically illustrated in Fig. 6.

The bending fatigue performance was evaluated through a quasi-static analytical approach, generating stress distribution and strain energy density fields. Comparative analysis in Fig. 7 juxtaposes the simulated von Mises stress contours with physical test evidence (Orientation 1). Simulation data revealed peak principal stress concentrations reaching 133.9 MPa at critical locations – 2.7% beyond the 130 MPa design threshold specified in the S-N curve parameters, thereby exceeding the critical material endurance limit and indicating structural failure under standardized bending fatigue protocols. Post-test examination confirmed crack initiation patterns conforming to bending fatigue failure mechanisms. Experimental fracture topography exhibited spatial correlation with computational stress hotspots, demonstrating the quantitative validity of the static-dynamic analogy methodology for wheel bending fatigue prediction.

It should be noted that regarding the fatigue evaluation, this study employs a rigorous engineering design criterion based on the equivalent stress threshold, rather than predicting the exact crack initiation life through full S-N curves. The primary objective is to verify whether the structural design strictly complies with the standard safety requirements by ensuring that the maximum localized stress remains well below the material's fatigue

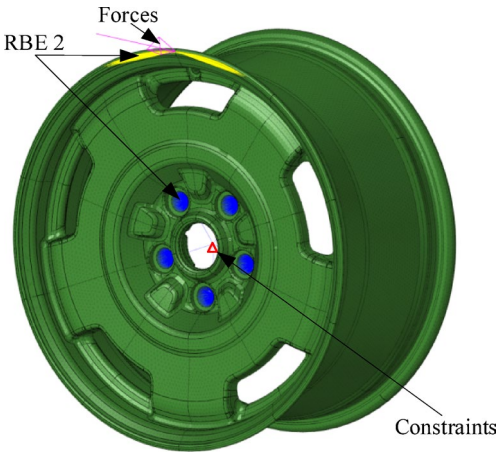

Fig. 8. The finite element model for 13° impact.

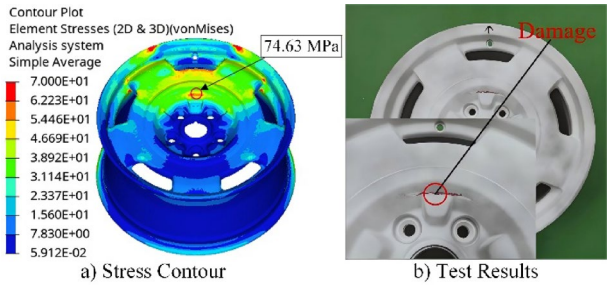

Fig. 9. 13° Impact simulation and test.

endurance limit. Under this infinite-life design framework, evaluating the peak equivalent stress inherently addresses the worst-case dynamic load cases.

The dynamic 13° impact simulation was transformed into an equivalent static load application at the impact cross-section to streamline the design process and improve optimization efficiency. The gravitational load (F_I) of the hammer was determined through the following equations:

$$F_I = Smg \tag{7}$$

where S denotes the equivalence factor of the simulated hammer system (1.1), and g indicates the gravitational acceleration (9.81 m/s^2).

The hammer's gravitational load (F_I) can be calculated as 7,445.8 N using the Eq. (7).

In accordance with the 13° impact test specifications for wheels, all DOFs at the nodes within the five bolt holes on the wheel mounting surface were fully constrained. RBE2 elements are utilized to simulate the bolted connection between the loading axle and the wheel mounting surface, with the central node of the RBE2 assembly constrained in all six DOFs. An additional RBE2 element group is implemented to couple nodes on the impact surface (flange region) to a centralized reference point, where a resultant force of 7445.8 N is applied normally to the impact plane, as illustrated in Fig. 8.

The 13° impact simulation was performed utilizing quasi-static analysis methodology, with computational outputs encompassing both von Mises stress distribution and strain energy fields. Figure 9 presents a comparative visualization of the simulated stress contour and experimental validation results. Numerical predictions revealed a maximum principal stress concentration of 74.63 MPa at the spoke-root region, exceeding the specified material failure criterion of 70 MPa. Consequently, structural integrity analysis confirmed non-compliance with 13° impact test requirements. Post-test examination of physical specimens demonstrated circumferential cracking patterns in the spoke area, correlating precisely with the finite element analysis prediction coordinates. Notably, the spatial congruence between computational stress hotspots and experimental fracture nucleation sites substantiates the validity of static simulation methodology for impact performance evaluation of wheel assemblies.

Single-load-case topology optimization setup

The original weight reduction cavities in the spoke back structure were filled using Altair HyperMesh software to reconstruct the wheel geometry, as illustrated in Fig. 10. Design space partitioning for the weight reduction cavities was performed following the specifications outlined in Sect. "Definition of the design domain". Adopting

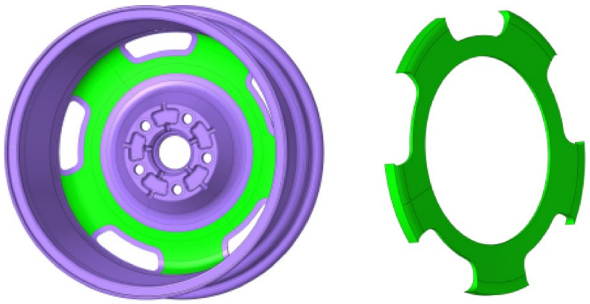

a) Wheel with weight reduction cavities filled

b) Filled Region

Fig. 10. Optimization model.

the variable-density method for topology optimization, a finite element model incorporating second-order tetrahedral elements was established. The refined mesh configuration consisted of 471,545 elements and 584,119 nodal points with a 5 mm characteristic element size. The designed domain consisted of 58,121 elements and 70,737 nodal points, while the non-designed domain comprised 413,424 elements and 513,382 nodal points.

Based on the wheel bending fatigue finite element model established in Sect. "Baseline performance evaluation and experimental validation", a topology optimization model for bending fatigue was constructed. Given that the load magnitudes in three orthogonal directions under the bending fatigue load case exhibit equivalence, structural compliance ($C_i(\rho)$) can be effectively computed through the weighted sum compliance method, as formulated in Eq. (8).

$$C_i(\rho) = \sum_{j=1}^{3} \lambda_{ij} C_{ij}(\rho) \tag{8}$$

where ρ denotes the material's relative density; i represents the load cases ($i=1,2$) with $i=1$ corresponding to bending fatigue and $i=2$ to 13°impact. Index j enumerates load components within the i-th load case ($j=1,2,3$); $C_{ij}(\rho)$ represents the compliance value in the j-th direction of the i-th load case; λ_{ij} denotes the weighting coefficient for the j-th direction of the i-th load case, with all directional weighting coefficients set to 0.33.

The topology optimization procedure was implemented in Altair OptiStruct, and the wheel spoke weight reduction cavities were designated as the design domain. The following manufacturing constraints were imposed: minimum member size control (10 mm) to eliminate checkerboard patterns; von Mises stress constraint (133.3 MPa) for structural integrity; draft angle constraint for casting manufacturability; and cyclical pattern grouping constraint with five rotational symmetry periods to maintain periodic topology.

The element density was set as the design variable, with the volume fraction response as the constraint condition and the minimization of weighted compliance as the objective function. Combining the mathematical model for topology optimization under the bending fatigue load case is as follows:

The element density was defined as the design variable, and the volume fraction constraint was imposed as the governing limitation. The minimization of weighted compliance is formulated as the objective function in bending fatigue or 13° impact load cases. Integrating the Eqs. (2) and (8), the topology optimization mathematical model under bending fatigue ($C_1(\rho)$) or 13° impact ($C_2(\rho)$) load cases is established as follows:

$$\begin{cases} \text{find } \rho = (\rho_1, \cdots, \rho_n) \\ \min C_1(\rho) = \sum_{j=1}^{3} 0.33 * C_{1j}(\rho) \\ \min C_2(\rho) = C_2(\rho) \\ \quad \text{subject to } K(\rho)U = P \\ \quad\quad V(\rho) \leqslant 0.5 \cdot V_0 \\ \quad\quad 0 = \rho_{\min} \leqslant \rho_i \leqslant 1 \\ \quad\quad \sigma_{\max} \leqslant 133.3 \text{ MPa} \end{cases} \tag{9}$$

It is important to note that the physical 13° impact test is a highly non-linear phenomenon involving transient dynamics and material plasticity. However, directly incorporating a full non-linear transient analysis within the SIMP topology optimization iterative loop is computationally prohibitive and prone to severe numerical instability. Therefore, consistent with widely accepted industrial design practices, a quasi-static equivalent load approach was adopted in this study. The transient impact energy was approximated as an equivalent peak static force applied to the rim flange. While this simplified linear-elastic SIMP method cannot capture post-yield material nonlinearity, it is highly effective at identifying the optimal load-transmission paths and maximizing global structural stiffness. By minimizing the structural compliance under this equivalent peak load, the resulting topology inherently exhibits enhanced resistance to dynamic impacts.

Manufacturing constraints and convergence analysis

In the topology optimization phase, the standard SIMP method is inherently susceptible to checkerboard effects and mesh dependency. To address these common numerical instabilities and ensure manufacturing feasibility, this study implemented specific filtering techniques through robust geometric constraints. Specifically, a minimum member size (MMS) of 10 mm was enforced. Within the utilized optimization solver, this MMS constraint mathematically functions as a sensitivity/density filter, which smooths the element sensitivities over a specified physical radius to explicitly prevent alternating solid-void patterns (checkerboarding) and guarantee mesh-independent results. Alongside this filtering approach, draft angle constraints for casting manufacturability and a cyclical pattern grouping constraint with five rotational symmetry periods were applied. These constraints effectively regulated the material distribution. As illustrated in Fig. 11, stable convergence was achieved in the optimization process. Following 15 iterations for the bending fatigue load case, the compliance values converged stably, ranging from 13,929.32 m/N to 17,075.71 m/N. Similarly, under the 13° impact load case, the compliance converged between 3,301.96 m/N and 3,925.04 m/N after 18 iterations, yielding a clear and manufacturable topological boundary.

Multi-load-case topology optimization via compromise programming

The topology optimization of wheels under bending fatigue and 13° impact load cases constitutes a Multi-Load-Case optimization problem with compliance minimization as the primary design criterion. Conventional Multi-Load-Case topology optimization methodologies typically employ linear weighting schemes to reduce the problem to a single-objective formulation. However, such scalarization techniques cannot ensure complete coverage of the Pareto frontier in non-convex optimization scenarios, as demonstrated in reference[32].

The compromise programming method[33] accounts for the effects of design variables on multiple objective functions through weighting coefficient allocation. By assigning appropriate weighting coefficients to individual objectives to balance their trade-offs, this methodology reformulates multi-objective optimization problems into scalar optimization formulations, thereby achieving mutually optimized relative solutions through simultaneous consideration of multiple objectives. The proposed approach integrates bending fatigue performance and 13° impact load cases through compromise programming, yielding a comprehensive evaluation function for spoke weight-reduction cavities[34] as expressed in the Eq. (10).

$$C(\rho) = \left\{ \sum_{i=1}^{2} \alpha_i^2 \left[\frac{C_i(\rho) - C_i^{\min}}{C_i^{\max} - C_i^{\min}} \right]^2 \right\}^{\frac{1}{2}} \tag{10}$$

where $C_i^{\max}$ and $C_i^{\min}$ denote the maximum and minimum compliance objective function values for the i-th load case, respectively; α_i represents the weighting coefficient of the i-th load case.

The weight coefficients of load cases were determined based on strain energy ratios across conditions, since strain energy serves as a reciprocal measure of structural stiffness. From strain energy outputs in Sect. "Optimization process and results discussion" 's finite element analysis, the wheel exhibited 1.389 MJ under bending fatigue and 0.510 MJ under 13° impact load cases. The weight coefficient ratio of the load case is formulated in the Eq. (11):

$$\alpha_1 : \alpha_2 = \frac{1}{1.389} : \frac{1}{0.510} \approx 0.27 : 0.73 \tag{11}$$

A topology optimization procedure was implemented in Altair OptiStruct, defining the spoke weight-reduction cavities as the design space. The optimization incorporated the following manufacturing-aware constraints:

(1) 10 mm minimum member size control (MMS) to mitigate checkerboard patterns;

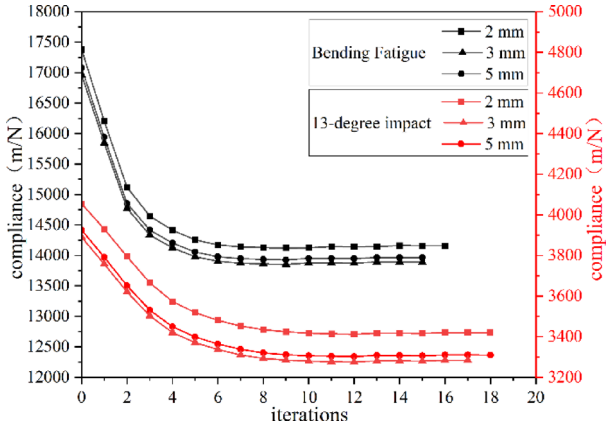

Fig. 11. Compliance convergence curve of single-load case topology optimization.

(2) 133.3 MPa allowable stress constraint ensuring structural integrity; As the criterion of 70 MPa for a 13° impact is smaller than the bending fatigue load case, the allowable stress of 133.3 MPa is uniformly used as the constraint value.

(3) geometric draft angle requirement to prevent material interference during mold release;

(4) pattern grouping configuration with five cyclic symmetry periods.

The Multi-Load-Case case optimization adopted minimization of a weighted compliance objective function employing element density as the design variable and volume fraction as the constraint parameter. This integrated optimization framework can be mathematically formulated by augmenting Eq. (2):

$$\begin{cases} \text{find } \rho = (\rho_1, \cdots, \rho_n) \\ \min\ C(\rho) = \left\{ \sum_{i=1}^{2} \alpha_i^2 \left[\frac{C_i(\rho) - C_i^{\min}}{C_i^{\max} - C_i^{\min}} \right]^2 \right\}^{\frac{1}{2}} \\ \quad \text{subject to } K(\rho)U = P \\ \quad\quad V(\rho) \leqslant 0.5 \cdot V_0 \\ \quad\quad 0 = \rho_{\min} \leqslant \rho_i \leqslant 1 \\ \quad\quad \sigma\max \leqslant 133.3 \text{ MPa} \end{cases} \tag{12}$$

The combined bending fatigue and 13° impact load cases were applied to establish the loads and boundary conditions for the Multi-Load-Case topology optimization, as shown in Fig. 12. For the 13° impact load case, RBE2 rigid coupling elements connected the wheel impact surface to a central reference point (RP). At the same time, the bolt holes were similarly linked to an RP at the wheel flange center via RBE2 constraints, fully constraining all degrees of freedom. For the bending fatigue load case, bolt connections between the loading shaft and wheel mounting surface are simulated using RBE2 elements, with tri-directional loads applied and all nodes along the inner rim periphery fully constrained.

After 138 iterations, the Multi-Load-Case topology optimization converged with an element density threshold of 0.3, revealing the optimal material distribution shown in Fig. 13. The figure illustrates the convergence history of the objective function and volume fraction, along with the evolution of material density distribution during the topology optimization process of the wheel. A comparison between the Multi-Load-Case optimization results in Fig. 13 and the initial wheel geometry shown in Fig. 1b reveals significant differences in the spoke lightening cavities. The original large-area shallow grooves have been replaced with localized deep cavities featuring a depth-wise gradient. This redesigned configuration enhances structural performance by optimizing load transmission paths, achieving an optimal balance between weight reduction and structural integrity.

This Multi-Load-Case topology optimization analysis was executed over 5.8 h using a 16-core CPU. In contrast to conventional design cycles often spanning multiple weeks, topology optimization offers a streamlined and time-efficient solution for designing wheel spoke weight-reduction cavities, significantly enhancing engineering productivity.

CAD reconstruction and mass reduction

After the Multi-Load-Case topology optimization converged, the main load-bearing path was extracted using a density threshold of 0.3, and the density field boundary was smoothed using OSSmooth. Then, the CAD reconstruction was completed by combining manufacturing constraints such as the minimum wall thickness of the spoke rear cavity, the draft angle, and the casting fillet. A reformed wheel geometry was successfully developed through parametric modeling driven by optimized dimensional parameters and integrated with pertinent manufacturing process design specifications, as illustrated in Fig. 14. Comparative mass analysis demonstrated a total mass reduction of 59 g, with the reconstructed configuration exhibiting 11.038 kg versus the initial design's 11.097 kg, equating to a 0.53% mass reduction ratio post-optimization. Crucially, to verify that this final smoothed and reconstructed CAD geometry maintains the performance predicted by the topology optimization, a secondary finite element validation was conducted. The verification confirmed that the reformed

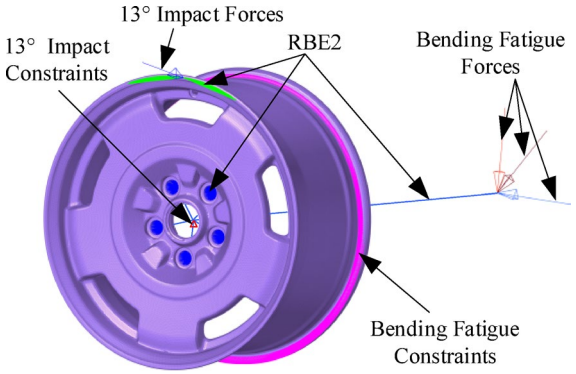

Fig. 12. Multi-load-case topology optimization model.

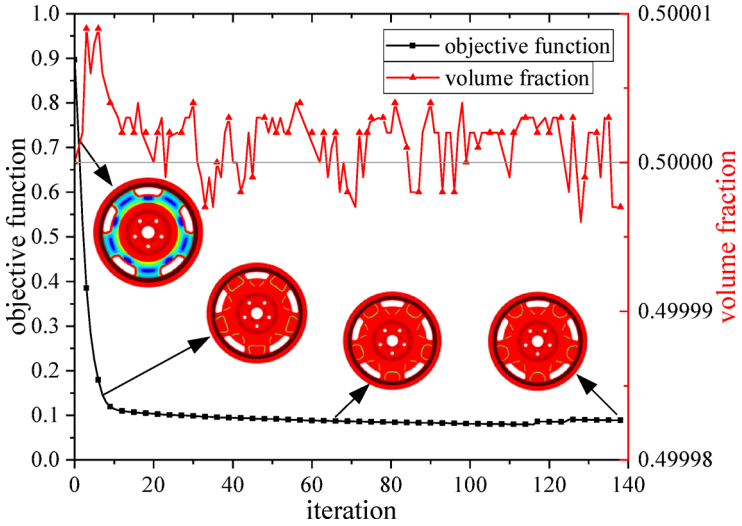

Fig. 13. Multi-load-case topology optimization results.

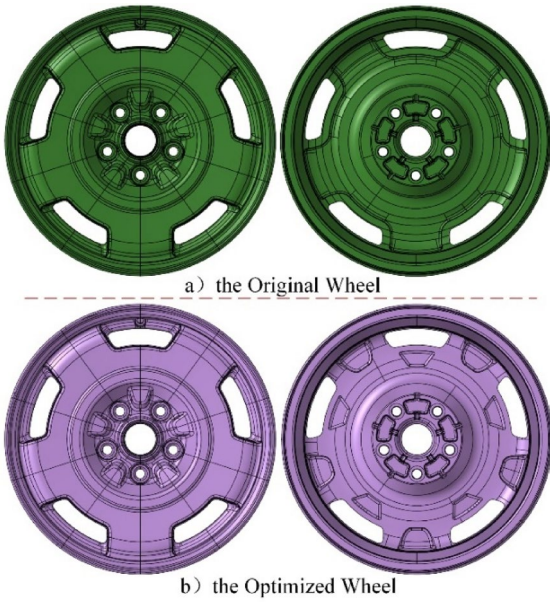

Fig. 14. Comparison of geometry before and after optimization.

model successfully retained the enhanced bending fatigue and impact resistance, ensuring structural integrity without any performance degradation induced by the CAD smoothing and reconstruction process.

Secondary FEA validation of the reconstructed wheel

Based on the bending fatigue finite element model detailed in Sect. "Baseline performance evaluation and experimental validation", the FEA model of the reconstructed wheel was developed, which contains 342,753 tetrahedral elements and 551,466 nodes after mesh discretization. The numerical simulation results in Fig. 15c demonstrate a peak von Mises stress of 108.13 MPa, significantly below the prescribed bending fatigue threshold of 130 MPa, fulfilling the structural integrity requirements.

Utilizing the 13° impact FE modeling methodology outlined in Sect. "Single-load-case topology optimization setup", a computational framework for analyzing the reconstructed wheel's dynamic response was established. As depicted in Fig. 15 d, the numerical simulations demonstrate maximum von Mises stress magnitudes reaching 63.76 MPa, maintaining a 9% safety margin relative to the established 70 MPa design allowable.

As summarized in Table 1, by utilizing the comprehensive evaluation function formulated through the compromise programming method as the objective function for topology optimization of spoke weight reduction cavities, the bending fatigue stress exhibited a 19.25% reduction. In comparison, the 13° impact stress demonstrated a 14.57% decrease. Notably, the original design's bending fatigue stress (133.9 MPa) and

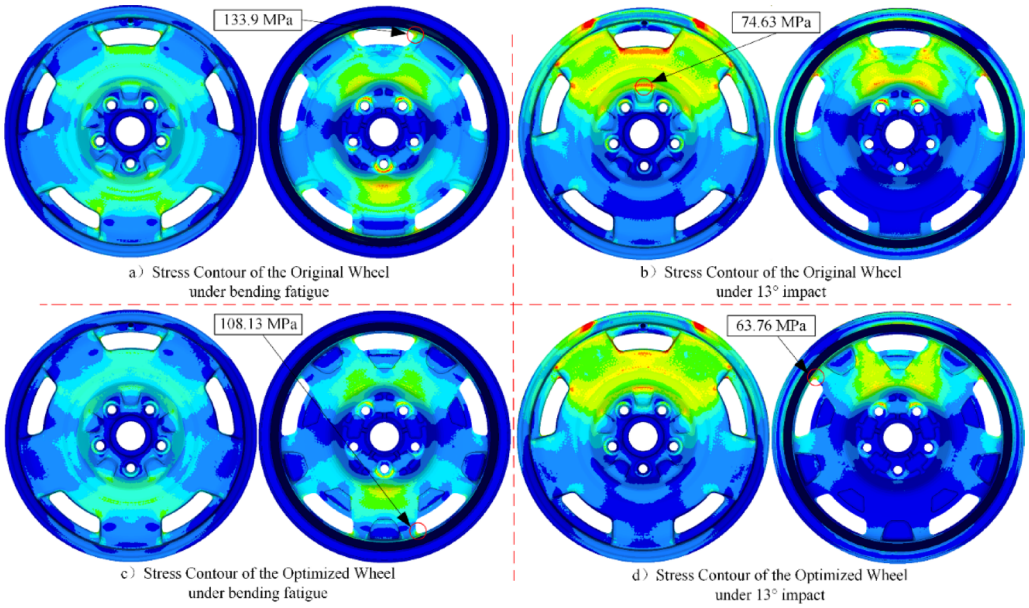

Fig. 15. Comparison of stress contours before and after optimization.

	Mass/kg	Criterion (11.5 kg)	Bending Fatigue/MPa	Criterion (130 MPa)	13° impact/MPa	Criterion (70 MPa)
Original wheel	11.097	OK (−3.5%)	133.9	NG	74.63	NG
Optimized wheel	11.038	OK (−4.0%)	108.13	OK	63.76	OK
Change	−0.53%		−19.25%		−14.57%	

Table 1. Comparison of performance before and after optimization.

13°-impact stress (74.63 MPa) exceeded respective specification thresholds (≤ 130 MPa and ≤ 70 MPa), whereas the optimized configuration achieves full compliance with certification requirements. The optimization process does not involve sacrificing one performance aspect in exchange for another. Instead, it achieves a more balanced compromise between the two load cases. This optimization process successfully transformed the non-compliant wheel into a compliant configuration meeting all design performance specifications.

Discussion

The Multi-Load-Case topology optimization framework proposed in this study effectively addresses the complex balance between lightweight design and structural integrity by revealing the underlying mechanism of material redistribution within wheel spoke cavities. Unlike conventional empirical designs that rely on fixed geometric configurations and broad, shallow grooves, the mathematically driven optimization reallocates material to form localized deep cavities with depth-wise gradients. This morphological transformation efficiently optimizes load transmission paths, significantly reducing the peak von Mises stress under bending fatigue load case by 19.25% (from 133.9 MPa to 108.13 MPa) and the 13° impact stress by 14.57% (from 74.63 MPa to 63.76 MPa). Consequently, a previously non-compliant baseline design was successfully converted into a fully compliant configuration.

To quantitatively evaluate the 'balanced' performance between fatigue and impact, a comparative analysis was conducted. While reconstructing a continuous Pareto frontier for this highly complex 3D topological space under exhaustive weight scanning is computationally prohibitive, the established comparative data clearly illustrates the balance relationship. Rather than sacrificing one performance metric to satisfy the other relative to the original design, the multi-objective approach, guided by the strain energy ratio, achieved simultaneous enhancements. Specifically, compared to the initial baseline, the optimized topology demonstrated an 18.4% improvement in bending fatigue stiffness (compliance reduced from 17,075.71 to 13,929.32 m/N) and a 14.3% improvement in 13° impact resistance (compliance reduced from 4,220.76 to 3,615.27 m/N). This explicitly indicates that the applied optimization strategy reached a highly reasonable structural compromise for both extreme load cases.

The engineering significance and novelty of this methodology are further highlighted when compared with existing literature on wheel topology optimization, as summarized in Table 2. Previous investigations have largely focused on static performance or single-physics scenarios. For instance, Zhang et al. and Xiao et al. primarily addressed static stiffness and modal frequencies, utilizing the entire spoke as the design domain while neglecting the evaluation of complex, synergistic load cases. While recent advances by Wang et al. and Kim et al.

Study	Design Domain	Load Cases/Objective	Key Features	Limitations
Zhang et al. 2012	Entire Spoke	Static Performance	Early wheel topology optimization validation	Limited load cases
Xiao et al. 2014	Entire Spoke	Stiffness + Modal	Multi-objective optimization	Does not emphasize shock/fatigue synergy
Wang et al. 2019	Entire Spoke	13°/90° Impact	Impact performance optimization	Lack of focus on shape preservation and manufacturability of rear cavity
Kim et al. 2022	Entire Spoke	Frequency + Mass	Combined topology and shape optimization	Does not address fatigue-impact balance
This Study	Rear Cavity of Spoke	Bending Fatigue + 13° Impact	Preserves outboard styling	Limited weight reduction, lacks full Pareto frontier construction

Table 2. Comparison of research on wheel spokes.

incorporated impact performance and frequency-mass optimization, they universally reconstructed the entire spoke morphology. This full-spoke approach inherently disregards the preservation of pre-existing, consumer-driven front-facing styling and the specific manufacturability constraints of the rear cavity. In contrast, the current study strictly confines the design domain to the spoke's rear cavity, preserving the aerodynamic front styling while achieving a balanced improvement in both bending fatigue and transient impact performance.

Transitioning theoretical topology optimization into practical industrial solutions presents significant challenges, particularly concerning conventional manufacturing techniques like gravity or low-pressure die casting. Unconstrained topology optimization often generates complex, organic geometries characterized by internal voids, checkerboard patterns, and severe undercuts, which are fundamentally unmanufacturable using traditional rigid molds. To bridge this gap between mathematical optimization and industrial production, this study embedded specific manufacturing-aware constraints directly into the optimization algorithm. Specifically, a minimum member size (MMS) control of 10 mm was applied to mitigate uncastable checkerboard patterns and ensure sufficient material thickness for structural rigidity. Furthermore, rigorous geometric draft angle requirements were imposed on the cavity design space. This ensures that the newly generated depth-gradient cavities do not cause material interference or die-locking during the mold release phase, making the optimized wheel immediately compatible with existing casting workflows without necessitating expensive additive manufacturing processes.

Despite the significant reduction in localized stress, this study presents several inherent limitations that must be fully acknowledged. First, regarding the mass reduction, the optimized wheel achieved only a marginal weight decrease of 0.53% (59 g). This limited reduction is the direct consequence of the strict region-constrained strategy. By confining the optimizable design domain exclusively to the spoke rear cavities to preserve the aerodynamic outboard styling, the algorithm was forced to prioritize the mitigation of severe stress concentrations over extreme lightweighting. This highlights a fundamental trade-off in industrial wheel redesign: preserving aesthetic integrity severely restricts the potential for substantial mass reduction.

Second, regarding the evaluation methodology, the current framework relies on a quasi-static equivalent load approach to simulate transient impact and dynamic fatigue. While this method efficiently guarantees safety through conservative stress thresholds, it cannot capture post-yield material nonlinearities during impact, nor can it precisely quantify explicit crack initiation cycles and long-term damage accumulation. Future research should integrate explicit transient dynamics and strain-life fatigue models for more comprehensive life predictions.

Conclusions

In this study, a Multi-Load-Case topology optimization framework was proposed to address the inherent limitations of empirical lightweight designs for aluminum alloy wheels. The main conclusions are drawn as follows:

(1) Targeting an 18 × 8.5 J aluminum alloy wheel, a Multi-Load-Case comprehensive evaluation function for spoke weight-reduction cavities was established. Through this strain-energy-based optimization, the peak von Mises stress was significantly reduced by 19.25% under the bending fatigue load case and by 14.57% under the 13° impact load case, alongside a marginal mass reduction of 0.53%. This confirms that the primary contribution of this region-constrained optimization lies in mitigating critical stress concentrations rather than achieving extreme lightweighting.

(2) Secondary finite element validation of the reconstructed wheel confirmed that its strength and stiffness fully comply with applicable regulatory specifications, successfully transforming a previously failing baseline into a safe and robust configuration.

(3) By strictly confining the topology design domain to the spoke rear cavities, this methodology effectively achieves the lightweight objectives without altering the original outboard styling. This region-constrained approach offers valuable guidance for the practical engineering design of wheel spokes.

(4) While the employed quasi-static equivalent method efficiently prevents fatigue failure via conservative stress thresholds, it cannot explicitly quantify crack initiation cycles. For future studies, integrating supplemental local stress-strain analysis or damage accumulation models is recommended for components requiring precise life predictions.

(5) Furthermore, regarding industrial scalability, the proposed Multi-Load-Case topology optimization framework exhibits significant potential for seamless integration into the standard wheel design cycle. By implementing this methodology during the early conceptual design phase, manufacturers can systematically replace traditional empirical trial-and-error iterations with a data-driven, automated structural generation

process. This integration not only significantly reduces product development time and physical prototyping costs but also ensures that the wheels strictly meet complex dynamic safety standards from the outset. Beyond automotive alloy wheels, this balanced optimization strategy can be readily scaled to other critical load-bearing components in the broader transportation sector, paving the way for advanced industrial applications.

Data availability

Data sets generated during the current study are available from the corresponding author on reasonable request.

Received: 5 February 2026; Accepted: 24 March 2026
Published online: 28 March 2026

References

1. Zhang, W. & Xu, J. Advanced lightweight materials for automobiles: A review. *Mater. Des.* **221**, 110994 (2022).
2. Li, J. et al. Research on the squeeze casting process of large wheel hub based on FEM and RSM. *Int. J. Adv. Manuf. Technol.* **128**(1), 197–208 (2023).
3. Jiang, Y. et al. Numerical simulation of billet height-diameter ratio on magnesium alloy automobile wheel formed by back extrusion[J]. *Int. J. Adv. Manuf. Technol.* **125** (1), 529–542 (2023).
4. Sigmund, O. & Maute, K. Topology optimization approaches: A comparative review. *Struct. multidisciplinary Optim.* **48** (6), 1031–1055 (2013).
5. Wu, J., Sigmund, O. & Groen, J. P. Topology optimization of multi-scale structures: A review. *Struct. Multidisciplinary Optim.* **63**(3), 1455–1480 (2021).
6. Deaton, J. D. & Grandhi, R. V. A survey of structural and multidisciplinary continuum topology optimization: Post 2000. *Struct. Multidiscip. Optim.* **49**(1), 1–38 (2014).
7. Van Dijk, N. P., Maute, K., Langelaar, M. & Van Keulen, F. Level-set methods for structural topology optimization: a review. *Struct. Multidisciplinary Optim.* **48** (3), 437–472 (2013).
8. Shin, S., Shin, D. & Kang, N. Topology optimization via machine learning and deep learning: A review. *J. Comput. Des. Eng.* **10**(4), 1736–1766 (2023).
9. Mukherjee, S. et al. Accelerating large-scale topology optimization: State-of-the-art and challenges. *Arch. Comput. Methods Eng.* **28**(7), 4549–4571 (2021).
10. Yvonnet, J. & Da, D. Topology optimization to fracture resistance: A review and recent developments. *Arch. Comput. Methods Eng.* **31**(4), 2295–2315 (2024).
11. Yousefpour, A. et al. Localized Physics-informed Gaussian Processes with Curriculum Training for Topology Optimization[J]. arXiv:2503.15561v1 [cs.LG], (2025).
12. Yousefpour, A. et al. Simultaneous and meshfree topology optimization with physics-informed Gaussian processes[J]. *Comput. Methods Appl. Mech. Eng.* **437**, 117698 (2025).
13. Zhang, Z. et al. Application of topological optimization on aluminum alloy automobile wheel designing[C]//Advanced Materials Research. *Trans. Tech. Publications*. **562**, 705–708 (2012).
14. Xiao, D. et al. Novel steel wheel design based on multi-objective topology optimization[J]. *J. Mech. Sci. Technol.* **28** (3), 1007–1016 (2014).
15. Wang, D., Zhang, S. & Xu, W. Multi-objective optimization design of wheel based on the performance of 13° and 90° impact tests. *Int. J. Crashworthiness* **24**(3), 336–361 (2019).
16. Kim, J., Kim, J. J. & Jang, I. G. Integrated topology and shape optimization of the five-spoke steel wheel to improve the natural frequency. *Struct. Multidisciplinary Optim.* **65**(3), 78 (2022).
17. Chu, D. et al. Research on Lightweight Technology of new carbon fiber wheel hub structure[J]. *IOP Conference Series: Earth and Environmental Science* **632**(5), 052071 (2021).
18. Zhang, Y. et al. An integrated multi-objective topology optimization method for automobile wheels made of lightweight materials. *Struct. Multidiscip. Optim.* **64**(3), 1585–1605 (2021).
19. Cascino, A., Meli, E. & Rindi, A. High-fidelity finite element modelling (FEM) and dynamic analysis of a hybrid aluminium–honeycomb railway vehicle carbody. *Appl. Sci.* **16**(1), 549 (2026).
20. Tang, J., Zhou, Z., Chen, H., Wang, S. & Gutiérrez, A. Research on the lightweight design of GFRP fabric pultrusion panels for railway vehicle. *Compos. Struct.* **286**, 115221 (2022).
21. Tang, J. et al. Laminate design, optimization, and testing of an innovative carbon fiber-reinforced composite sandwich panel for high-speed train. *Polym. Compos.* **42**(11), 5811–5829 (2021).
22. Cascino, A., Meli, E. & Rindi, A. Design and optimization of a hybrid railcar structure with multilayer composite panels. *Materials* **18**(21), 5013 (2025).
23. Luo, R. K., Gabbitas, B. L. & Brickle, B. V. Fatigue life evaluation of a railway vehicle bogie using an integrated dynamic simulation. *Proc. Inst. Mech. Eng. Part F J. Rail Rapid Transit* **208**, 123–132 (1994).
24. Luo, R. K., Gabbitas, B. L. & Brickle, B. V. Dynamic stress analysis of an open-shaped railway bogie frame. *Eng. Fail. Anal.* **3**(1), 53–64 (1996).
25. Suzuki, K. & Kikuchi, N. A homogenization method for shape and topology optimization. *Comput. Methods Appl. Mech. Eng.* **93**(3), 291–318 (1991).
26. Xie, Y. M. et al. Recent Developments in Evolutionary Structural Optimization (ESO) and Bidirectional ESO (BESO). *Adv. Mech.* **41** (4), 462–471 (2011).
27. Sethian, J. A. & Wiegmann, A. Structural boundary design via level set and immersed interface methods. *J. Comput. Phys.* **163**(2), 489–528 (2000).
28. Mlejnek, H. P. & Schirrmacher, R. Engineer's approach to optimal material distribution and shape finding[J]. *Comput. Methods Appl. Mech. Eng.* **106** (1–2), 1–26 (1993).
29. Rietz, A. Sufficiency of a finite exponent in SIMP (power law) methods[J]. *Struct. Multidisciplinary Optim.* **21** (2), 159–163 (2001).
30. National Technical Committee of Auto Standardization. *GB/T 5334 – 2021: Performance Requirements and Test Methods for Passenger Car Wheel Bending and Radial Fatigue* (Standards Press of China, 2021).
31. National Technical Committee of Auto Standardization. *GB/T 15704 – 2012: Road Vehicles—Impact Test Method for Light Alloy Wheels* (Standards Press of China, 2013).
32. Min, S., Nishiwaki, S. & Kikuchi, N. Unified topology design of static and vibrating structures using multiobjective optimization. *Computers & Structures* **75**(1), 93–116 (2000).
33. Chen, W., Wiecek, M. M. & Zhang, J. Quality utility - a compromise programming approach to robust design[J]. *J. Mech. Des. Trans. ASME.* **121** (2), 179–187 (1999).
34. Wang, Z. H. Key Technologies for Lightweight Design of Aluminum Alloy Wheel Hub Structures. Ph.D. Thesis, Yanshan University, (2022).

Author contributions

Guangdong Zhang contributed towards conceptualization, methodology, validation, supervision, and writing—Review & Editing. Xin Cui contributed towards analysis, validation, and writing original draft. Yongxing Zang, Yangyang Zhou, Jianjun Lu, Zhansheng Li, Haitao Yang, JianDong Wang, ZhenYe, Risheng Li, and Linzhen Zhou contributed towards conceptualisation, methodology, supervision, and writing—Review & Editing.

Funding

This work is supported by the Hebei Province Innovation Capacity Improvement Plan Project (Grant No. 24431003D), the Central Guidance on Local Science and Technology Development Fund of Hebei Province (Grant No. 254Z1009G).

Declarations

Competing interests

The authors declare no competing interests.

Additional information

Correspondence and requests for materials should be addressed to G.Z. or Y.Z.